Int. J. Res. Ind. Eng. Vol. 7, No. 1 (2018) 84–105

International Journal of Research in Industrial Engineering
www.riejournal.com

Unsteady Magnetohydrodynamic Stagnation Point Flow of a Nanofluid over a Slendering Stretching Sheet Using Buongiorno's Model

G.Vinod Kumar, R.V. M. S. S Kiran Kumar*, S.V. K. Varma
Department of Mathematics, S.V. University, Tirupati-517502, A.P, India.

A B S T R A C T

This paper aimed to model and analyze the unsteady hydromagnetic boundary layer stagnation point nanofluid flow over a non-linear stretching surface through porous medium with variable wall thickness. The effects of radiation, dissipation, and slip velocity are taken into account. The formulation of the problem is made through Buongiorno's model, which involves the aspects of thermophoresis and Brownian motion. The set of governing non-linear Ordinary Differential Equations (ODE's) are solved numerically by using boundary value problem default solver in MATLAB bvp4c package. The impact of different flow quantities on fluid velocity, temperature, and nanoparticle concentration are analyzed and examined through graphs. The physical parameters like friction factor coefficient $(-F''(0))$, rates of heat transfer $(-\Theta'(0))$, and nanoparticle friction $(-\Phi'(0))$ are derived and presented through tables. It is found that the wall thickness parameter (α) depreciates the nanofluid velocity for $n<1$ and accelerates when $n>1$. Also, the unsteadiness parameter shows a significant effect on the stagnation point flow.

Keywords: Magneticfield, Stagnation point, Unsteady nanofluid flow, Wall thickness, Partial slip.

Article history: *Received: 26 October 2017* *Accepted: 19 February 2018*

1. Introduction

A point in which the local velocity of the fluid is zero is called a stagnation point. Basically, stagnation point exists at the surface of objects in the flow field, wherever the fluid is brought to rest by the substance. Hiemenz [1] pioneered the flow of a stagnation point in a plane. He examined the stagnation flow problem over a stationary plate and used alikeness transformations to convert the Navier–Stokes equations into non-linear Ordinary Differential Equations (ODE's). Several researchers have spread the idea to consider various aspects of the stagnation point flows. Due to its various practical applications, the stagnation point flow attracting many researchers. The above-mentioned applications include microelectronics cooling, emergency core cooling

* Corresponding author
E-mail address: rsai.maths@gmail.com, kksaisiva@gmail.com
DOI: 10.22105/riej.2018.102367.1028

systems, and the ice chiller in Air-Conditioning systems (AC's), wire drawing, polymer extrusion, etc.

In many engineering and industrial process, the flow over a stretching sheet having tremendous applications, for example, melt-spinning, the hot rolling, extrusion, wire drawing, manufacture of glass -fiber, plastic and rubber sheets production, large metallic plates cooling in a bath, etc. Polymer sheets and filaments in industries are fabricated by unremitting extrusion of the polymer from a die to a windup roller and are placed at a finite distance away. Crane [2] originated the study of flow over a stretching sheet. In this problem, he solved a steady 2D flow over a linearly stretching plate analytically. Later, Wang [3] extended the idea of Crane from two-dimensional to three-dimensional case. Suali et al. [4] discussed the suction and injection effects on stagnation point flow past a stretching/shrinking sheet and concluded that the mass suction causes to increment of range of dual solutions while the opposite trend is observed for mass injection. Also, few useful recent investigations about stagnation point flows over a stretching surface have been reported in the Refs [5-8].

Nanofluids are the advanced category of heat transfer fluids, and are the mixture of nanoparticles and base fluids and nanoparticles. Nanofluids have been exposed to enhance the thermal conductivity as well as convective heat transfer rate of the base fluids. The size of nanoparticle is a microscopic and its range is between 1-100 nm. Nowadays, the research with nanoparticles is a new class of intense scientific interest because of a wide diversity of inherent applications in optical, biomedical, electronic fields, etc. Firstly, in 1995, Choi [9] and Khanafer et al. [10] investigated the performance of heat transfer in nanofluids inside an enclosure taking into account the solid particle diffusion. The improvement of thermal conductivity of conventional heat transfer fluids by adding micro-sized solid particles is a relatively new development in engineering and technology. The added particles are able to enhance the thermal conductivity and heat transfer rate due to the base fluids have lower thermal conductivity than solid metals. Buongiorno [11] gave the comprehensive survey on convective transport in nanofluids and he observed the abnormal increase of the thermal conductivity of nanofluids.

The MHD stagnation point flow of a water-based nanofluid adjacent to a linearly stretching/shrinking porous sheet was discussed by Khalili et al. [12]. The stagnation point flow of carbon-water nanofluid past a stretched cylinder in the presence of velocity slip and thermal radiation is considered by Hayat et al. [13]. They observed the higher heat transfer for increasing values of curvature parameter. Hady et al. [14] reported the hydromagnetic stagnation point slip flow of a nanofluid over a linearly stretching porous sheet in the presence of thermal radiation. Salem et al. [15] analyzed the unsteady hydro stagnation point flow of a water based copper nanofluid in the presence of radiation. The boundary layer radiative nanofluid flow over a heated stretching surface by considering unsteady free stream condition was reported by Das et al. [16]. Rizwan Ul Haq et al. [17] considered the influence of radiation and thermal slip on hydrodynamic stagnation-point nanofluid flow over a stretching surface. Akbar et al. [18] considered the hydromagnetic stagnation point flow of radiative a nanofluid over a stretching surface with

convective type boundary condition. Nagendramma et al. [19] studied the stagnation point flow of Maxwell nanofluid over a stretched surface with viscous dissipation and radiation. Recently, Hayat et al. [20] examined the unsteady stagnation point flow of Maxwell nanofluid over an impermeable stretched surface with thermal radiation. Farooq et al. [21] investigated the MHD stagnation point flow of viscoelastic nanofluid over a stretching surface with convective boundary condition and thermal radiation. Kiran Kumar and Varma [22] investigated the hydromagnetic nanofluid slip flow in a porous medium over a non-linear stretching sheet under the influence of thermal radiation, heat source, and first order chemical reaction. Das [23] analyzed the slip flow a nanofluid over a permeable non-linear stretching surface at prescribed surface temperature.

In general, the stretching/shrinking sheets need not be flat. Thus, sheets with variable wall thickness can be encountered more often in real world applications. Such types of sheets are often used in machine design, architecture, nuclear reactor technology, naval structures, and acoustical components. Variable wall thickness is one of the important properties in the analysis of vibration of orthotropic plates. The concepts of variable thickness sheets originated through linearly deforming substance such as needles and nozzles. Lee [24] originated the idea about the variable thickness sheet. Later, boundary layer stretching sheet flow with variable thickness is studied by Fang et al. [25]. The MHD Ag-water and TiO_2-water nanofluids flow over a stretching sheet with variable wall thickness was considered by Acharya et al. [26] and found that the nanofluid temperature reduced with increase in the wall thickness parameter. The non-linear MHD nanofluid flow with variable wall thickness is analyzed by Prasad et al. [27] and concluded that the flow decelerated with suction and accelerated with increasing injection. Kiran Kumar and Varma [28] investigated the magnetohydrodynamic nanofluid flow through porous medium over a slendering sheet under the influence of viscous dissipation, thermal radiation and first order chemical reaction, and found that radiation and thermophoresis parameters enhanced the nanofluid temperature. Recently, the hydrodynamic hyperbolic nanofluid flow over a stretching sheet with variable wall thickness was discussed by Hayat et al. [29]. The MHD stagnation point flow over a stretching surface by using Cattaneo-Christov heat flux model with variable thermal conductivity was studied by Hayat et al. [30].

The main purpose of the current study is to examine the effects of thermophoresis, Brownian motion, radiation, velocity slip, and dissipation on an unsteady hydromagnetic stagnation point flow of a nanofluid past a stretching surface through porous medium with variable wall thickness. The governing non-linear equations are solved by using default solver in MATLAB bvp4c package. The impact of a mixture of pertinent flow quantities are discussed through graphs and tables.

1. Mathematical Formulation

We consider an unsteady, two dimensional hydromagnetic stagnation point flow of a nanofluid over a non-linear stretching sheet with variable wall thickness under the influence of variable

magnetic field, variable porous permeability, partial velocity slip, radiation, and dissipation effects. The stretching sheet motion is chosen in the $x-$axis, and the $y-$axis is taken perpendicular to it. The stretching sheet velocity as well as free stream velocity are chosen as $u_w(x,t)=\frac{a(x+b)^n}{1-\lambda t}$, and $U_\infty(x,t)=\frac{c(x+b)^n}{1-\lambda t}$ where $\lambda t<1$, λ is unsteadiness frequency parameter, t is time, a, c are constants, b denotes the physical quantity related to sheet, and n is velocity exponent/power index parameter. We assume that the sheet is not flat and is defined as $y=E(x+b)^{\frac{1-n}{2}}$ $(n\neq 1)$; E is a very small constant so that the sheet is adequately thin to avoid a measurable pressure gradient along the sheet $\left(\frac{\partial p}{\partial x}=0\right)$. The flow is caused due to stretching sheet. The radiative heat flux is described by using Rosseland approximation. The wall is not-permeable with $v_w=0$. A magnetic field of strength B_0 is applied perpendicular to the flow direction. We assume that the present analysis is valid only for $n\neq 1$, since for $n=1$ the problem reduces to a flat sheet. It is assumed that the induced magnetic field is neglected due to small magnetic Reynolds. The Hall current and electric field effects are neglected. The joule heating is neglected and viscous dissipation effect is taken into account. The Buongiorno's model which involves the aspects of Brownian motion and thermophoresis is used.

Under aforesaid assumptions, the time dependent governing boundary layer equations for the Buongiorno's nanofluid model are (see [31, 32]):

$$\frac{\partial u}{\partial x}+\frac{\partial v}{\partial y}=0, \tag{1}$$

$$\frac{\partial u}{\partial t}+u\frac{\partial u}{\partial x}+v\frac{\partial u}{\partial y}=\frac{\partial U_\infty}{\partial t}+U_\infty\frac{\partial U_\infty}{\partial x}+\upsilon\frac{\partial^2 u}{\partial y^2}-\frac{\sigma B^2(x,t)(u-U_\infty)}{\rho}-\frac{\upsilon(u-U_\infty)}{k^1} \tag{2}$$

$$\frac{\partial T}{\partial t}+u\frac{\partial T}{\partial x}+v\frac{\partial T}{\partial y}=\alpha\frac{\partial^2 T}{\partial y^2}+\tau\left\{D_B\frac{\partial C}{\partial y}\frac{\partial T}{\partial y}+\frac{DT}{T_\infty}\left(\frac{\partial T}{\partial y}\right)^2\right\}+\frac{\upsilon}{c_p}\left(\frac{\partial u}{\partial y}\right)^2-\frac{1}{(\rho c_p)}\frac{\partial q_r}{\partial y} \tag{3}$$

$$\frac{\partial C}{\partial t}+u\frac{\partial C}{\partial x}+v\frac{\partial C}{\partial y}=D_B\frac{\partial^2 C}{\partial y^2}+\frac{D_T}{T_\infty}\frac{\partial^2 T}{\partial y^2}. \tag{4}$$

The related boundary conditions are:

$$u\left(x,E\sqrt{\frac{(x+b)^{1-n}}{1-\lambda t}}\right)=u_w+S_1\frac{\partial u}{\partial y},\ v\left(x,E\sqrt{\frac{(x+b)^{1-n}}{1-\lambda t}}\right)=0,\ T\left(x,E\sqrt{\frac{(x+b)^{1-n}}{1-\lambda t}}\right)=T_w(x,t),$$

$$C\left(x,E\sqrt{\frac{(x+b)^{1-n}}{1-\lambda t}}\right)=C_w(x,t)\ (n\neq 1),$$

$$u\to U_\infty(x,t), T\to T_\infty(x,t)\ C\to C_\infty(x,t)\ \text{as}\ y\to\infty. \tag{5}$$

Here (u,v) are the velocity components along the (x,y) axis, respectively. The υ denotes the kinematic viscosity, c_p represents the specific heat at constant pressure, ρ is the base fluid density, α_m denotes the thermal diffusivity, τ is the heat capacity ratio, D_B for the Brownian diffusion coefficient and D_T for the thermophoresis diffusion coefficient. $T_{w,}, C_w$ are the wall temperature and nanoparticle concentration, respectively, and $T_{\infty,}, C_\infty$ are the free steam temperature and nanoparticle concentration, respectively.

The slip coefficient S_1 is assumed as

$$S_1 = \sqrt{\frac{(x+b)^{1-n}}{1-\lambda t}}. \tag{6}$$

Also, we assumed that the special forms for an unsteady flow

$$B(x,t) = B_0\sqrt{\frac{(x+b)^{n-1}}{1-\lambda t}},\quad k = k',\frac{(x+b)^{1-n}}{1-\lambda t},\quad T_w(x,t) = T_\infty + T_0\sqrt{\frac{(x+b)^{1-n}}{1-\lambda t}},$$
$$C_w(x,t) = C_\infty + C_0\sqrt{\frac{(x+b)^{1-n}}{1-\lambda t}}. \tag{7}$$

The Rosseland radiative heat flux q_r is:

$$q_r = \frac{-4\sigma^*}{3k^*}\frac{\partial T^4}{\partial y}, \tag{8}$$

where k^* and σ^* denote the mean absorption coefficient and the Stefan-Boltzmann constant, respectively, and the linear temperature function T^4 is expanded by using Taylors series expansion in terms of T_∞ as

$$T^4 = 4TT_\infty^3 - 3T_\infty^4. \tag{9}$$

In the view of Eq. (8) and Eq. (9), the Eq. (3) can be reduced as

$$\frac{\partial T}{\partial t} + u\frac{\partial T}{\partial x} + v\frac{\partial T}{\partial y} = \alpha\frac{\partial^2 T}{\partial y^2} + \tau\left\{D_B\frac{\partial C}{\partial y}\frac{\partial T}{\partial y} + \frac{DT}{T_\infty}\left(\frac{\partial T}{\partial y}\right)^2\right\} + \frac{\upsilon}{c_p}\left(\frac{\partial u}{\partial y}\right)^2 + \frac{16\sigma^* T_\infty^3}{3(\rho C_P)k^*}\frac{\partial^2 T}{\partial y^2}. \tag{10}$$

2. Similarity Transformations and Solution of the Problem

For mathematical analysis, we describe the following dimensionless similarity transformations:

$$\eta = y\sqrt{a\frac{(n+1)}{2\nu}\left(\frac{(x+b)^{n-1}}{(1-\lambda t)}\right)}, u = \frac{a(x+b)^n}{1-\lambda t}f',$$

$$v = -\sqrt{a\frac{(n+1)}{2}\nu(x+b)^{n-1}}\left[f + \eta\left(\frac{n-1}{n+1}\right)f'\right]$$
$$\theta(\eta) = \frac{T - T_\infty}{T_w(x,t) - T_\infty}, \quad \psi(\eta) = \frac{C - C_\infty}{C_w(x,t) - C_\infty}. \tag{11}$$

In view of above suitable variables, the governing boundary layer equations and related boundary conditions (2-5) can be written as follows:

$$f''' + ff'' - \frac{2A}{(n+1)}\left(f' + \frac{\eta}{2}f'' - A_1\right) - \left(\frac{2n}{n+1}\right)f'^2 + \left(M + \frac{1}{K}\right)(A_1 - f') + A_1^2\left(\frac{2n}{n+1}\right) = 0, \tag{12}$$

$$\frac{1}{\Pr}\left(1 + \frac{4R}{3}\right)\theta'' + Nb\phi'\theta' + Nt\theta'^2 - \frac{A\eta}{(n+1)}\theta' + Ecf''^2 + f\theta' = 0, \tag{13}$$

$$\psi'' + Scf\psi' + \frac{Nt}{Nb}\theta'' - \frac{A\eta Sc}{(n+1)}\psi' = 0. \tag{14}$$

$$f(\alpha) = \alpha\left(\frac{1-n}{1+n}\right)\left[1 + Sf''(\alpha)\right], f'(\alpha) = 1 + Sf''(\alpha), \theta(\alpha) = 1, \psi(\alpha) = 1$$
$$f'(\infty) = A_1, \theta(\infty) = 0, \psi(\infty) = 0. \tag{15}$$

where $\alpha = E\sqrt{\frac{a(n+1)}{2\upsilon}}$ is the wall thickness parameter and $S = \sqrt{\frac{a(n+1)}{2\upsilon}}$ is the velocity slip parameter. Equations (12-14) with boundary conditions (15) are non-linear equations defined on a domain $[\alpha, \infty)$. In order to assist the computation and change the domain to become $[0, \infty)$. Also, we define a new function, $F(\xi) = F(\eta - \alpha) = f(\eta)$, $\Theta(\xi) = \Theta(\eta - \alpha) = \theta(\eta)$ and $\Phi(\xi) = \Phi(\eta - \alpha) = \psi(\eta)$. Therefore, the Equations (12-14) and boundary conditions (15) become

$$F''' + FF'' - \frac{2A}{(n+1)}\left(F' + \frac{\eta}{2}F'' - A_1\right) - \left(\frac{2n}{n+1}\right)F'^2 + \left(M + \frac{1}{K}\right)(A_1 - F') + A_1^2\left(\frac{2n}{n+1}\right) = 0, \tag{16}$$

$$\frac{1}{\Pr}\left(1 + \frac{4R}{3}\right)\Theta'' + Nb\Phi'\Theta' + Nt\Theta'^2 - \frac{A\eta}{(n+1)}\Theta' + EcF''^2 + F\Theta' = 0, \tag{17}$$

$$\Phi'' + ScF\Phi' + \frac{Nt}{Nb}\Theta'' - \frac{A\eta Sc}{(n+1)}\Phi' = 0. \tag{18}$$

$$F(0) = \alpha\left(\frac{1-n}{1+n}\right)\left[1 + SF''(0)\right], F'(0) = 1 + SF''(0), \Theta(0) = 1, \ \Phi(0) = 1$$
$$F'(\infty) = A_1, \ \Theta(\infty) = 0, \ \Phi(\infty) = 0. \tag{19}$$

$\Pr = \frac{\upsilon}{\alpha}$ is the Prandtl number, $Sc = \frac{\upsilon}{D_B}$ for Lewis number, $Nb = \frac{\tau D_B (C_w - C_\infty)}{\upsilon}$ is the non-dimensional Brownian motion parameter, $Nt = \frac{\tau D_T (T_w - T_\infty)}{T_\infty \upsilon}$ is the non-dimensional thermophoresis parameter, $M = \frac{2\sigma B_0^2}{a(n+1)\rho}$ is the magnetic field parameter, $Ec = \frac{u_w^2}{c_p (T_w - T_\infty)}$ is the

Eckert number, $A=\frac{\lambda(x+b)^{1-n}}{a}$ is the unsteadiness parameter, $A_1=\frac{c}{a}$ is the velocity ratio parameter, $R=\frac{4\sigma^* T_\infty^{\ 3}}{kk^*}$ for thermal radiation parameter and $K=\frac{a(1+n)k}{2\upsilon}$ is the permeability parameter.

For the sake of engineering, the skin friction coefficient (Cf), the rate of heat (Nu_x) and mass (Sh_x) transfer coefficients are defined as

$$\frac{Cf}{\mathrm{Re}_x^{-\frac{1}{2}}}=-2\sqrt{\frac{n+1}{2}}F''(0),\ \frac{Nu_x}{\mathrm{Re}_x^{-\frac{1}{2}}}=-\sqrt{\frac{n+1}{2}}\Theta'(0),\ \frac{Sh_x}{\mathrm{Re}_x^{-\frac{1}{2}}}=-\sqrt{\frac{n+1}{2}}\Phi'(0), \tag{20}$$

where $\mathrm{Re}_x=\frac{u_w(x+b)}{\upsilon}$ is the local Reynolds number.

3. Numerical Procedure

In this section, we present a numerical procedure of the above boundary value problem. In general, a Boundary Value Problem (BVP) consists of a set of Ordinary Differential Equations (ODE's), some boundary conditions, and a guesses that includes which solution is desire.

The procedure for the present problem is

$$F'''=-\left(FF''-\frac{2A}{(n+1)}\left(F'+\frac{\eta}{2}F''-A_1\right)-\left(\frac{2n}{n+1}\right)F'^2+\left(M+\frac{1}{K}\right)(A_1-F')+A_1^{\ 2}\left(\frac{2n}{n+1}\right)\right),$$

$$\Theta''=-\frac{\mathrm{Pr}}{\left(1+\frac{4R}{3}\right)}\left(Nb\Phi'\Theta'+Nt\Theta'^2-\frac{A\eta}{(n+1)}\Theta'+EcF''^2+F\Theta'\right),$$

$$\Phi''=-\left(Sc\,F\Phi'+\frac{Nt}{Nb}\Theta''-\frac{A\eta Sc}{(n+1)}\Phi'\right).$$

Subject to the boundary conditions

$$F(0)=\alpha\left(\frac{1-n}{1+n}\right)\left[1+SF''(0)\right],\ F'(0)=1+SF''(0),\Theta(0)=1,\quad \Phi(0)=1$$
$$F'(\infty)=A_1,\ \Theta(\infty)=0,\ \Phi(\infty)=0. \tag{21}$$

We can choose the guess in the following form (see [33]):

$$u(x,t)=u_w+S_1\frac{\partial u}{\partial y},$$
$$v(x,t)=0,$$
$$T(x,t)=T_w(x,t),$$
$$C(x,t)=C_w(x,t),$$
$$u(x,t)=U_\infty(x,t),$$

$$T(x,t)=T_{\infty}(x,t),$$
$$C(x,t)=C_{\infty}(x,t).$$

To solve this problem with bvp4c, we provide functions that evaluate the differential equations and the residual in the boundary conditions. These functions must return column vectors with components of f corresponding to the original variables as $f(1)=F$, $f(2)=F'$, $f(3)=F''$, $f(4)=\Theta$, $f(5)=\Theta'$, $f(6)=\Phi$ and $f(7)=\Phi'$. These functions can be coded in MATLAB as

```
function dydx = exlode(x,f)
dydx =  [f(2)
          f(3)
           -(((M+(1/K))*(A1-f(2)))-((2*A/(n+1))*(f(2)+(0.5*n1*f(3)-
A1)))-(((2*n)/(n+1))*(f(2)*f(2)))+(f(1)*f(3))+((A1*A1)*(2*n)/(n+1)))
            f(5)
            -(3/(3+(4*R)))*((Pr*Nb*f(5)*f(7))+(Pr*Nt*f(5)*f(5))-
(Pr*A*n1*f(5)/(n+1))+(Pr*f(1)*f(5))+(Pr*Ec*f(3)*f(3)))
            f(7)
           -((Le*f(1)*f(7))-((A*Le*n1*f(7))/(n+1))+((Nt/Nb)*(-
(3/(3+(4*R)))*((Pr*Nb*f(5)*f(7))+(Pr*Nt*f(5)*f(5))-
(Pr*A*n1*f(5)/(n+1))+(Pr*f(1)*f(5))+(Pr*Ec*f(3)*f(3))))))];

function res = exlbc(fa,fb)
res = [ fa(1)-(a*((1-n)/(1+n)))*(1+(S*fa(3)))
       fa(2)-(1+(S*fa(3)))
       fa(4)-1
       fa(6)-1
       fb(2)-A1
       fb(4)
       fb(6)];
```

The guess is supplied to bvp4c in the form of a structure. Whereas the name *solinit* will be used in this problem, we treat as solution of initial value problem. However, it must contain two fields that must be called *x* and *f*. A guess for a mesh that reveals the behavior of the solution is provided as the vector *solinit.x*. A guess for the solution at these mesh points is provided as the array *solinit.y* with each column *solinit.f (:, i)* approximating the solution at the point *solinit.x(i)*. It is not difficult to form a guess structure, but a helper function *bvpinit* makes it easy in the most common circumstances. It creates the structure when given the mesh and a guess for the solution in the form of a constant vector or the name of a function for evaluating the guess.

The guess structure is then developed with *bvpint* by

```
solinit = bvpinit(linspace(0, 1, infinity), @exlinit);
```

The boundary value problem has now been defined by means of functions for evaluating the differential equations and the boundary conditions and a structure providing a guess for the solution. When default value are used, that is all you need to solve the problem with bvp4c:

```
sol = bvp4c(@shootode,@shootbc,solinit);
```

The output of bvp4c is a structure called here sol. The mesh determined by the code is returned as *sol.x* and the numerical solution approximated at these mesh points is returned as *f=sol.y.* As the guess, *sol.f* (:, i) approximates the solution at the point *sol.x(i).*

4. Results and Discussions

The set of non-linear Ordinary Differential Equations (ODE's), (16-18), with the associated boundary conditions (19) are solved numerically by using boundary value problem default solver in MATLAB bvp4c package. The obtained results are presented and analyzed with the help of graphs and tables. For numerical calculation, we fixed the values of dimensionless parameters as

$$M = 1,\ A = 0.1,\ n = 0.1, Pr = 0.71,\ \alpha = 0.3, S = 0.5,\ \eta = 0.1, Nb = 0.2,\ Ec = 0.1, R = 0.3,$$

$$Nt = 0.5, Sc = 2, A_1 = 1.$$

Figure 1 describes the impact of magneticfield parameter (*M)* on velocity distribution. It is seen that the fluid velocity is a decreasing function of *M.* This is because the existence of magnetic field sets in a resistive force called Lorentz force, which is a retarding force on the velocity field; consequently, the velocity is reduced. From this, we concluded that the magnetic field may play an important role to control the velocity and heat transfer in the various conducting fluids. Figure 2 reveals the impact of porosity parameter (*K)* on $F'(\eta)$. It is seen that the fluid velocity $(F'(\eta))$ decrease with the rising values of *K*. This is because the porous medium results into a drag force (i.e. Darcy force) which decelerates the fluid velocity within the hydromagnetic boundary layer. Figures 3-5 describe the variation of wall thickness parameter (α) on nanofluid velocity, nanofluid temperature, and nanoparticle concentration distributions. It is noted that the velocity of the fluid decreases with the increasing α for $n<1$. Also, the momentum boundary layer thickness becomes thinner for higher value of α when $n<1$. Meanwhile the velocity of the fluid increases monotonically from the surface to the ambient fluid as α increases for $n>1$. Because of the boundary condition $\left(\text{i.e. } F(0)=\alpha\left(\frac{1-n}{1+n}\right)\left[1+SF''(0)\right]\right)$, for $\text{n}=2$, we have $F(0)<0$, i.e. mass injection and for $n=0.5$ we have $F(0)>0$ that represents mass suction at the wall. Figure 1 shows the flow, temperature, and concentration fields are significantly decreases for suction while it is increases for injection. Further, all the three boundary layers thickness decreases for $n=0.5$ but improved for $\text{n}=2$.

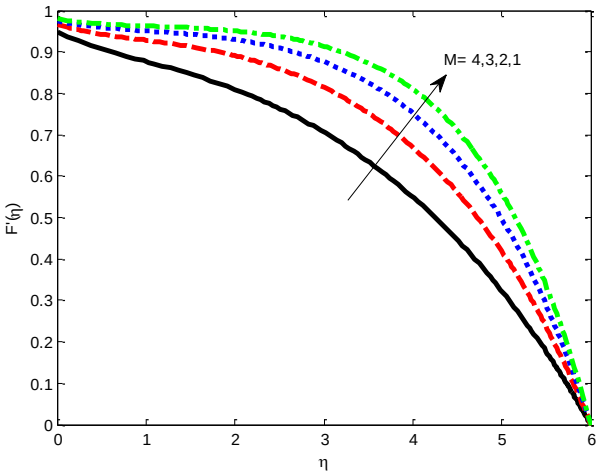

Figure 1. Effect of M on $F'(\eta)$.

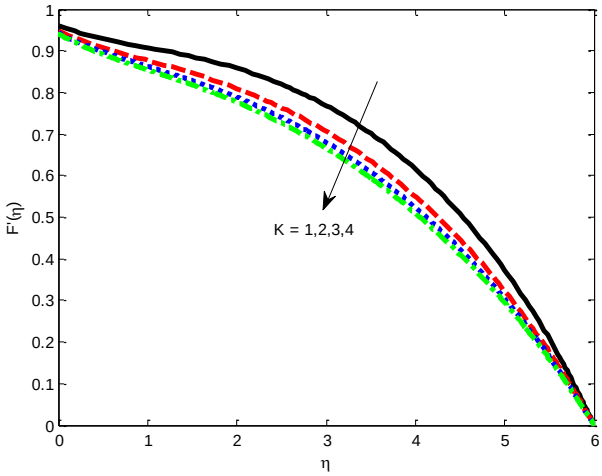

Figure 2. Effect of K on $F'(\eta)$.

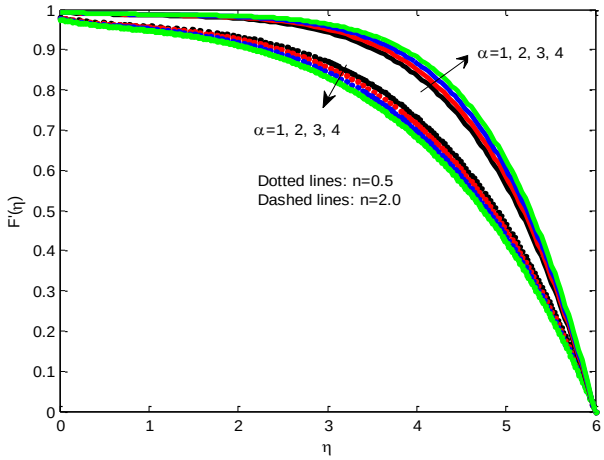

Figure 3. Effect of α on $F'(\eta)$.

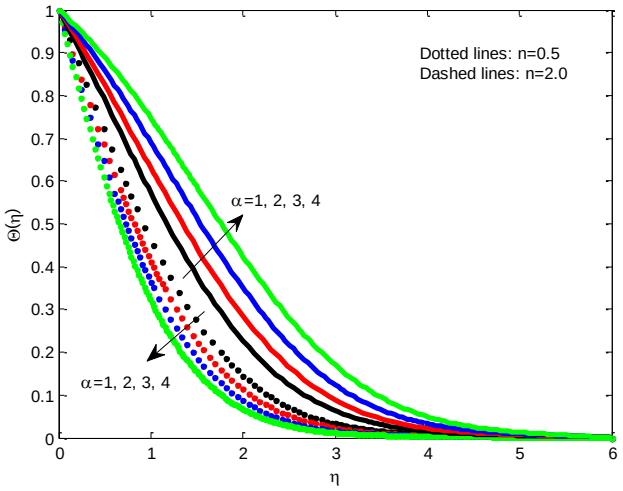

Figure 4. Effect of α on $\Theta(\eta)$.

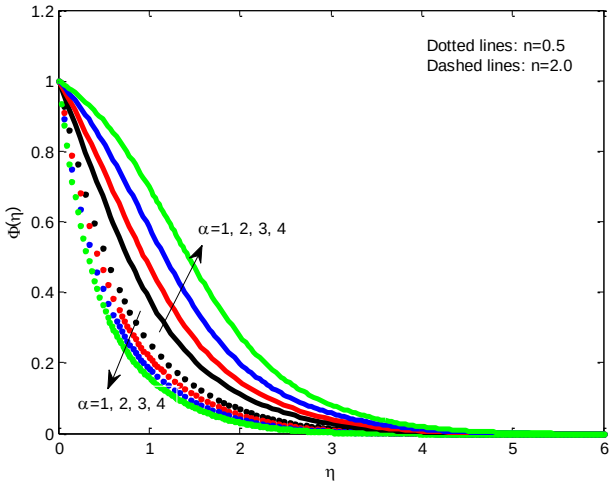

Figure 5. Effect of α on $\Phi(\eta)$.

Figures 6-8 demonstrate the outcome of an unsteady parameter (*A)* on velocity, temperature, and concentration fields. It is observed that the velocity along the stretching sheet decline with the increase in *A*. Likewise, the thickness of the boundary layer becomes thinner for a larger value of *A*. Physically, it means that the temperature gradient at the sheet increases while *A* increases, which implies the increase in heat transfer rate at the surface. This shows an important fact that the rate of cooling is much faster for higher values of unsteadiness parameter, where it may take a longer time in steady flows.

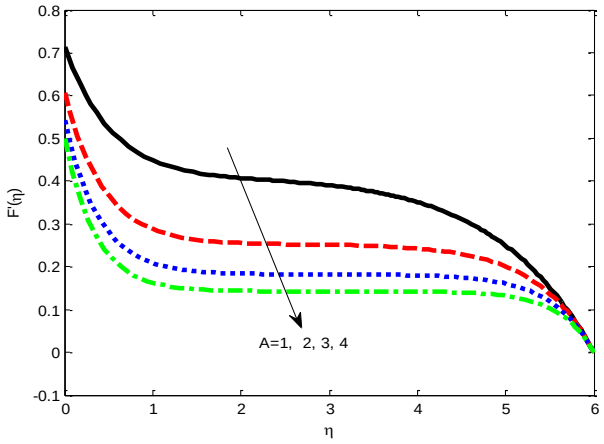

Figure 6. Effect of A on $F'(\eta)$.

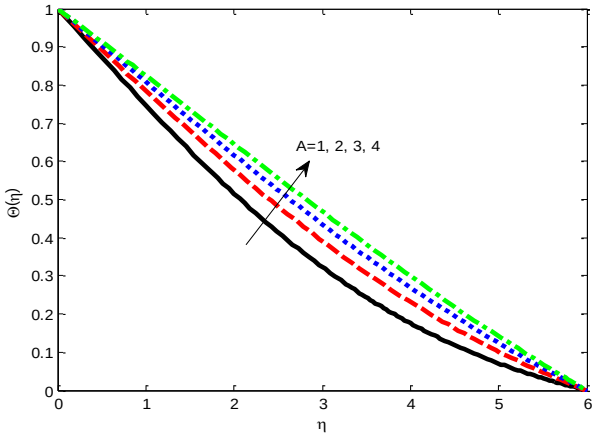

Figure 7. Effect of A on $\Theta(\eta)$.

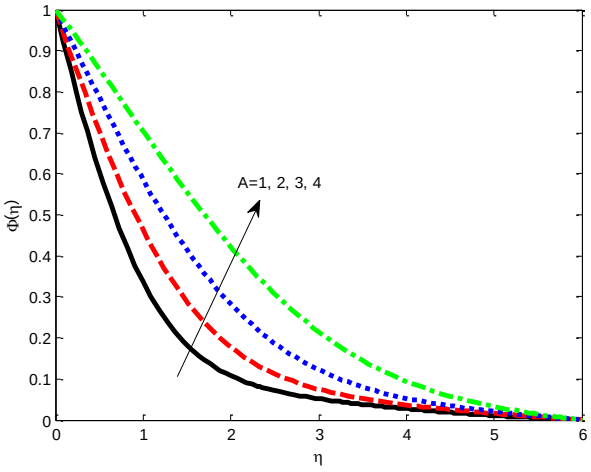

Figure 8. Effect of A on $\Phi(\eta)$.

Figures 9-11 reveal the effect of slip parameter (S) on fluid velocity, temperature, and nanoparticle concentration distributions. It is clear that as S increases, the slip at the surface wall raises, and reaches to a smaller amount of penetration due to the stretching surface into the fluid. Also, we observed that the velocity component at the wall decreases with the rising values of slip parameter. Therefore, the hydromagnetic boundary layer thickness decreases with the rising values of S. While by escalating S, thermal and solutal boundary layer thickness enhances. Figures 12 and 13 display the effect of Brownian motion parameter (Nb) on temperature and nanoparticle concentration fields. It is clear that the Brownian motion leads to the temperature distribution increasing and the nanoparticle concentration fields decreasing, because the larger Nb corresponds to stronger random motion of nanoparticles within a fluid. Subsequently, the fluid temperature and its boundary layer thickness enhances. Also, the nanoparticle concentration gradient at the wall is forbidden passively at the surface by product of $-\left(\frac{Nt}{Nb}\right)$ and temperature gradient.

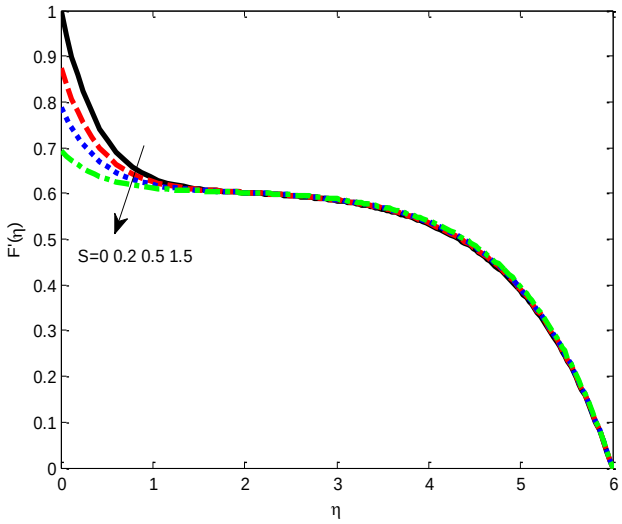

Figure 9. Effect of S on $F'(\eta)$.

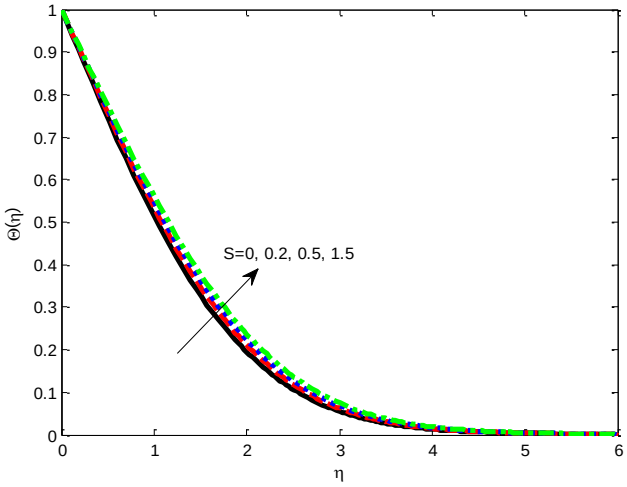

Figure 10. Effect of S on $\Theta(\eta)$.

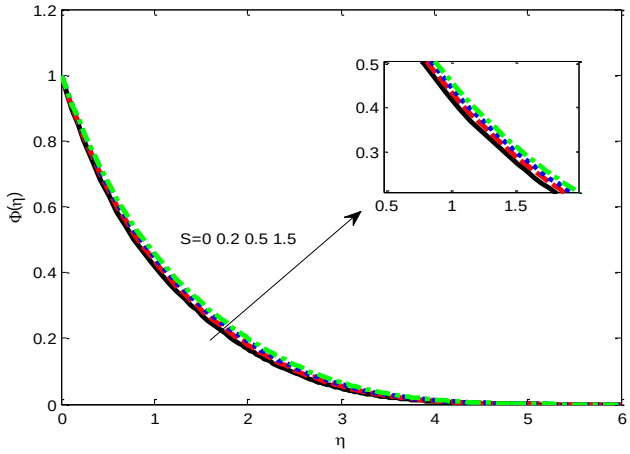

Figure 11. Effect of S on $\Phi(\eta)$.

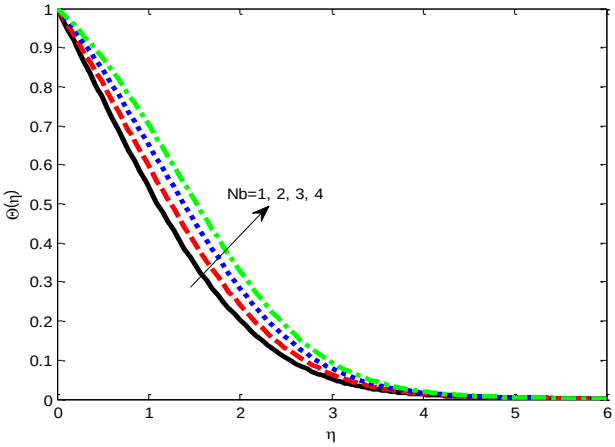

Figure 12. Effect of Nb on $\Theta(\eta)$.

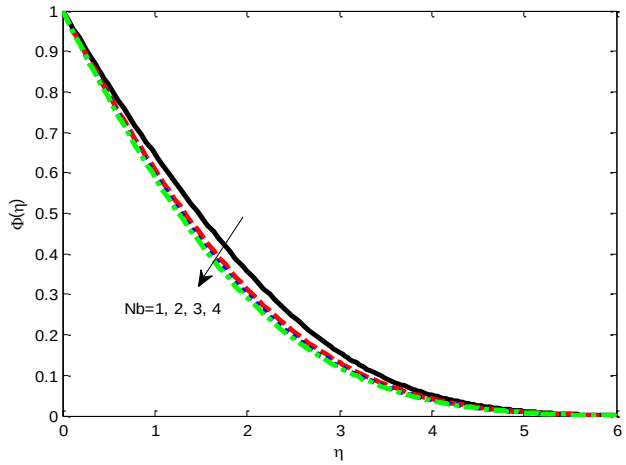

Figure 13. Effect of Nb on $\Phi(\eta)$.

The impact of thermophoresis parameter (Nt) on temperature and nanoparticle concentration fields is shown in Figures 14 and 15. Physically, the thermophoresis is a mechanism in which tiny particles are dragging away from hot surface to cold surface. Due to this transportation, the fluid temperature increases. Also, the thermophoretic effect corresponds to the larger mass flux, which significantly increases the nanoparticle concentration. The effect of velocity power index parameter (n) on the velocity field is plotted in Figure16. It is seen that the hydromagnetic boundary layer thickness become thicker as n increases along the stretching surface. Physically, a variation in the values of n means stretching the sheet linearly, quadratically, cubically, etc. Figure 17 demonstrates that the improving values of radiation parameter (R) accelerates the nanofluid temperature. It is noted that the presence of radiation parameter leads to developing of the thermal boundary-layer. Physically, increasing the radiation parameter produces a significant increase in the thermal boundary layer thickness. In fact, the radiation parameter decreases the fluid temperature. While the radiation parameter increases, the mean Rosseland absorption co-efficient k^* decreases. Hence, the thermal radiation factor is better suitable for cooling process.

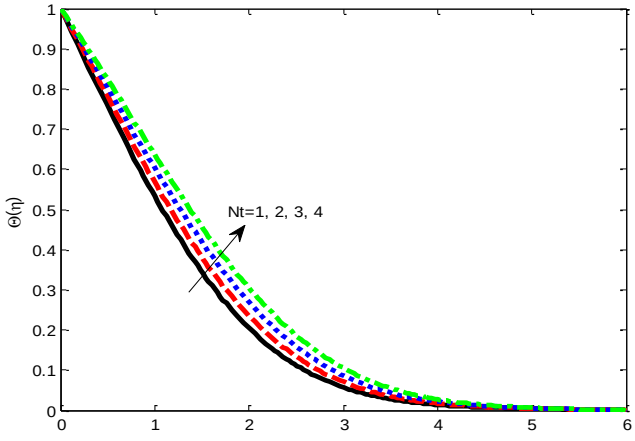

Figure 14. Effect of Nt on $\Theta(\eta)$.

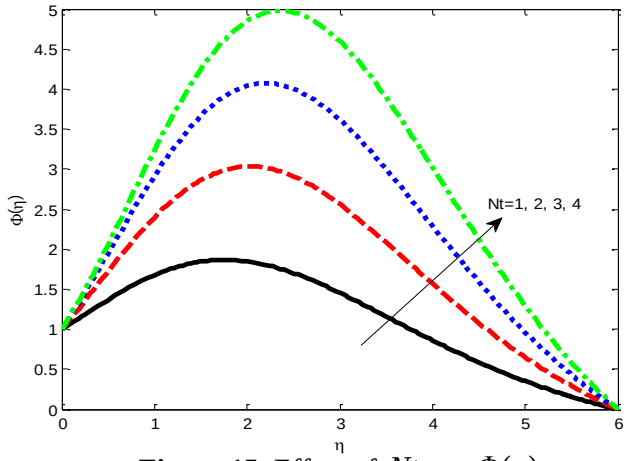

Figure 15. Effect of Nt on $\Phi(\eta)$.

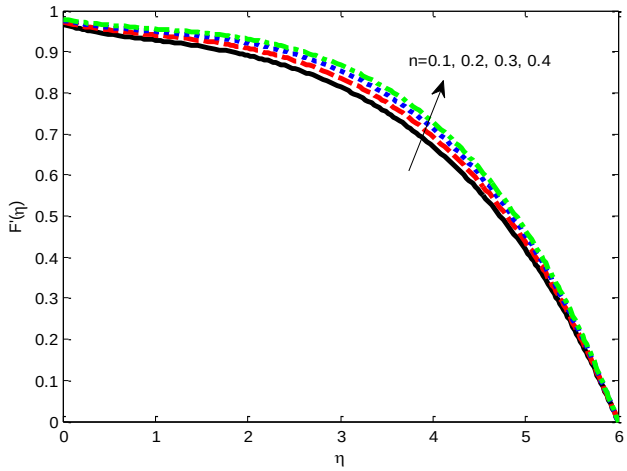

Figure 16. Effect of n on $F'(\eta)$.

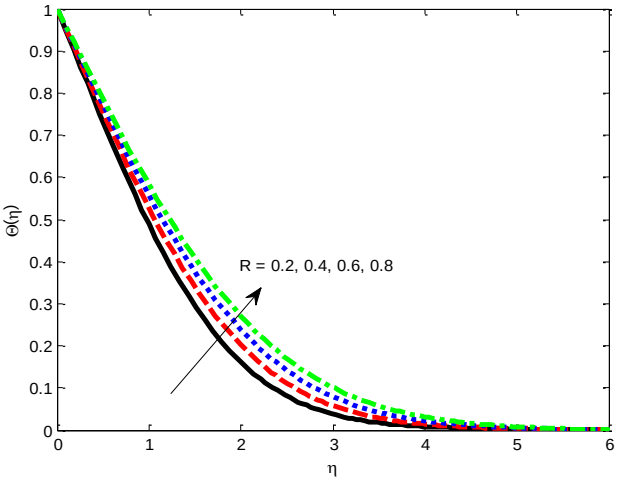

Figure 17. Effect of R on $\Theta(\eta)$.

Figure 18 demonstrates the impact of Eckert number (Ec) on temperature profiles. The ratio between advective transports and heat dissipation potential is called Eckert number (Ec);

therefore, advective transport is proportional to Eckert number. Hence, for large values of *Ec* the nanofluid temperature is increased significantly. The rising values of *Sc* depreciate the nanoparticle concentration, which is shown in Figure 19. The ratio between viscosity and molecular diffusivity is termed as Schmidt number $\left(Sc = \frac{\upsilon}{D_B} \right)$. Therefore, for large value of *Sc*, the thickness of thermal boundary layer is larger than the thickness of nanoparticle boundary layer.

Table 1 illustrates the numerical results of different flow quantities on the friction factor coefficient $-(F''(0))$, the rates of heat transfer $-(\Theta'(0))$ and nanoparticle friction $-(\Phi'(0))$ coefficients. It is observed that increasing the values of permeability parameter (K), wall thickness parameter (α) and unsteadiness parameter (A) improves the friction factor coefficient while the reverse phenomena rises values of power index parameter (n), velocity slip parameter (S) and magnetic field parameter (M). Also, the heat transfer rate is decreases with the rising values of permeability parameter (K), Brownian motion parameter (Nb), unsteadiness parameter (A), thermophoresis parameter (Nt), radiation parameter (R), Eckert number (Ec), power index parameter (n) and velocity slip parameter (S); whereas it increases with M and α. Furthermore, the nanoparticle friction increases with improving values of M, α, Nb, R, Ec and decreases with n, K, A, Nt and S. It is also noted that the S leads to a depreciation in the friction factor coefficient; when slip occurs, the flow velocity near the sheet is no longer equal to the stretching surface velocity. The similar phenomenon is observed on the local Nusselt number and local nanoparticle fraction coefficient. The Nt, Nb, R and Ec show no effect on friction factor coefficient.

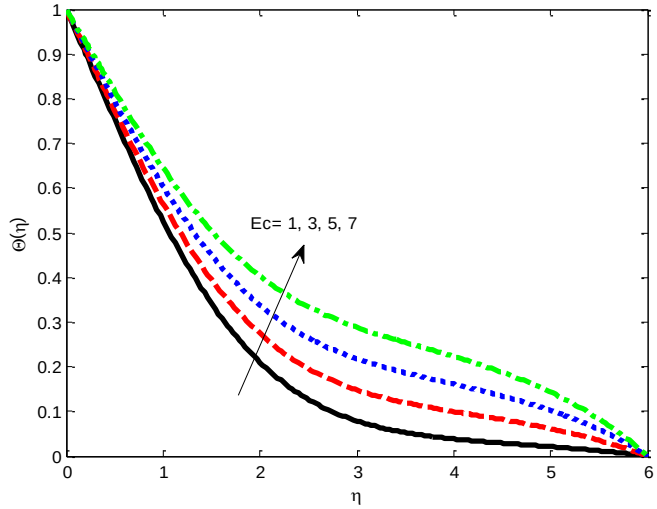

Figure 18. Effect of Ec on $\Theta(\eta)$.

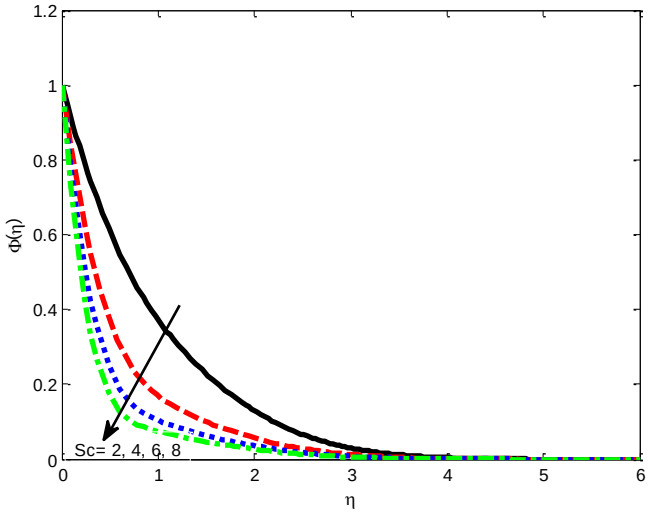

Figure 19. Effect of Sc on $\Phi(\eta)$.

5. Comparison of Results and Error Analysis

In this section, we provide the correctness of our results with the existing results of Ibrahim et al. [34], Mahapatra and Gupta [35], and Bhattacharyya [36]. Also, we find the Errors and Relative Errors with respect to the existing results. In this calculation, Error means the difference between the present value and exact value, and the relative error is the ratio of error to exact value. Table 2 and 3 presents the numerical comparison of present results between the existing results of Ibrahim [34], Mahapatra [35], and Bhattacharyya [36]. From this computation, it is noticed that our results and the numerical method are very good agreement with the existing numerical (see [34] and [35]), analytical results (see [36]) and results in some limiting cases. Also, we observed that the error bound in this case is very small and is guaranteed by further supporting the present results with existing results.

Table 1. Numerical values of $-F''(0)$, $-\Theta'(0)$ and $-\Phi'(0)$ for various flow parameter.

M	K	α	A	Nb	Nt	R	Ec	n	S	$-F''(0)$	$-\Theta'(0)$	$-\Phi'(0)$
1	2	0.3	0.1	0.2	0.5	0.3	0.1	0.1	0.5	0.102327	0.336145	1.240813
2										0.066085	0.345771	1.263218
3										0.049777	0.350265	1.273259
	1									0.102327	0.360021	1.232658
	2									0.103586	0.352344	1.204119
	3									0.115103	0.348878	1.190660
		0.1								0.199861	0.389186	1.024754
		0.5								0.231186	0.416128	1.367078
		1.5								0.272035	0.449967	1.821460
			0.5							0.411613	0.384465	1.040512
			1.5							0.699745	0.354184	0.759103
			2.0							0.788494	0.343631	0.652004
				0.5						0.215319	0.384746	1.265057
				1.5						0.215319	0.330064	1.296363
				2.0						0.215319	0.305399	1.299911
					0.5					0.215319	0.395348	1.138706
					1.5					0.215319	0.360933	1.134560
					2.0					0.215319	0.344897	1.121616
						1				0.215319	0.441848	1.136635
						3				0.215319	0.384150	1.219812
						5				0.215319	0.366438	1.246463
							0.5			0.215319	0.395141	1.204589
							1.5			0.215319	0.376412	1.234604
							2.0			0.215319	0.367043	1.249617
								0.5		0.114479	0.399234	1.090406
								1.5		0.053882	0.390271	0.949588
								2.0		0.043774	0.387530	0.912886
									0.3	0.262635	0.404165	1.210673
									0.5	0.215319	0.402631	1.192588
									0.7	0.182597	0.401540	1.179952

Table 2. Comparison of the numerical values of $f''(0)$ for M=0, A=0, n=1, Pr=1, α=0, S=0, $K \to \infty$.

A_1	Ibrahim et al. [34]	Mahapatra and Gupta [35]	Bhattacharyya [36]	Present results	Error	Relative Error
0.01	-0.9980	-	-	-0.999197	-0.001197	0.0012
0.1	-0.9694	-0.9694	−0.969386	-0.969656	-0.000256	0.00026
0.2	-0.9181	-0.9181	-0.918107	-0.918165	-0.000065	0.00007
0.5	-0.6673	-0.6673	-0.667263	-0.667264	0.000036	0.00005
2.0	2.0175	2.0175	2.017503	2.017503	0.000003	0.0000015
3.0	4.7292	4.2793	4.729284	4.729282	0.000082	0.000020

Table 3. Comparison of the numerical values of $-\theta'(0)$ for , A=0, n=1, Pr=1, α=0 , S=0, K $\to\infty$, Nt=0, Nb=0, R=0, Ec=0 .

Pr	A_1	Ibrahim et al. [34	Mahapatra and Gupta [35]	Present results	Error	Relative error
1	0.1	0.6022	0.603	0.602812	0.000612	0.00102
	0.2	0.6245	0.625	0.624655	0.000155	0.00025
	0.5	0.6924	0.692	0.692452	0.000052	0.00008
1.5	0.1	0.7678	0.777	0.776812	0.000013	0.00002
	0.2	0.7971	0.797	0.797126	0.000026	0.00003
	0.5	0.8648	0.863	0.864794	-0.000006	-0.00001

6. Concluding Remarks

The flow of problems over a stretching sheet play a vital role in many engineering process with its incredible applications. With this intension, an attempt was made to investigate the unsteady stagnation point nanofluid flow over a stretching sheet in a porous medium with variable wall thickness. The combined effects of Brownian motion and thermophoresis were considered by the Buongiorno's model. The impact of various flow of parameters was discussed through graphs and tables.

- The strength of thermophoresis decreased for smaller nanoparticles, so that the smaller nanoparticles were able to build up at the heated wall and improve the heat transfer rate.
- The slip parameter reduced the transfer rates from the stretching sheet to the fluid.
- The increment in radiation parameter caused to reduce the surface temperature gradient and increase in radiation parameter, and hence the heat transfer rate from the surface decreased with increasing R. However, it enhanced the fluid temperature.
- The pulling of the stretching surface can be only partly transferred to the fluid. Due to this reason, the fluid velocity decreased with the slip condition.
- The wall thickness parameter increased the fluid velocity monotonically when $n>1$, while a reverse phenomenon was observed for $n<1$.
- The results showed the substantial impact of the aforementioned unsteady parameter on fluid velocity, temperature, and nanoparticle concentration fields.

References

[1] Hiemenz, K. (1911). Die Grenzschicht an einem in den gleichformigen Flussigkeitsstrom eingetauchten geraden kreiszylinder. Gottingen dissertation. *Dingler's polytech. J*, *326*, 311.

[2] Crane, L. J. (1970). Flow past a stretching plate. *Zeitschrift für angewandte mathematik und physik zamp*, *21*(4), 645-647.

[3] Wang, C. Y. (1984). The three-dimensional flow due to a stretching flat surface. *The physics of fluids*, *27*(8), 1915-1917.

[4] Suali, M., Nik Long, N. M. A., & Ariffin, N. M. (2012). Unsteady stagnation point flow and heat transfer over a stretching/shrinking sheet with suction or injection. *Journal of applied mathematics*, *2012*.

[5] Zhong, Y., & Fang, T. (2011). Unsteady stagnation-point flow over a plate moving along the direction of flow impingement. *International journal of heat and mass transfer*, *54*(15-16), 3103-3108.
[6] Ishak, A., Jafar, K., Nazar, R., & Pop, I. (2009). MHD stagnation point flow towards a stretching sheet. *Physica A: Statistical mechanics and its applications*, *388*(17), 3377-3383.
[7] Hayat, T., Qayyum, S., Alsaedi, A., & Waqas, M. (2016). Simultaneous influences of mixed convection and nonlinear thermal radiation in stagnation point flow of Oldroyd-B fluid towards an unsteady convectively heated stretched surface. *Journal of molecular liquids*, *224*, 811-817.
[8] Hayat, T., Khan, M. I., Tamoor, M., Waqas, M., & Alsaedi, A. (2017). Numerical simulation of heat transfer in MHD stagnation point flow of Cross fluid model towards a stretched surface. *Results in physics*, *7*, 1824-1827.
[9] Choi, S. U., & Eastman, J. A. (1995). Enhancing thermal conductivity of fluids with nanoparticles. *Proceedings of the ASME international mechanical engineering congress and Exposition*, 66. Argonne National Lab., IL (United States).
[10] Khanafer, K., Vafai, K., & Lightstone, M. (2003). Buoyancy-driven heat transfer enhancement in a two-dimensional enclosure utilizing nanofluids. *International journal of heat and mass transfer*, *46*(19), 3639-3653.
[11] Buongiorno, J. (2006). Convective transport in nanofluids. *Journal of heat transfer*, *128*(3), 240-250.
[12] Khalili, S., Dinarvand, S., Hosseini, R., Tamim, H., & Pop, I. (2014). Unsteady MHD flow and heat transfer near stagnation point over a stretching/shrinking sheet in porous medium filled with a nanofluid. *Chinese physics B*, *23*(4), 048203.
[13] Hayat, T., Khan, M. I., Waqas, M., Alsaedi, A., & Farooq, M. (2017). Numerical simulation for melting heat transfer and radiation effects in stagnation point flow of carbon–water nanofluid. *Computer methods in applied mechanics and engineering*, *315*, 1011-1024.
[14] Hady, F. M., Eid, M. R., & Ahmed, M. A. (2014). Slip effects on unsteady MHD stagnation point flow of a nanofluid over stretching sheet in a porous medium with thermal radiation. *Journal of pure and applied mathematics: Advances and applications*, *12*(2), 181-206.
[15] Salem, A. M., Ismail, G., & Fathy, R. (2015). Unsteady MHD boundary layer stagnation point flow with heat and mass transfer in nanofluid in the presence of mass fluid suction and thermal radiation. *The European physical journal plus*, *130*(6), 113.
[16] Das, K., Duari, P. R., & Kundu, P. K. (2014). Nanofluid flow over an unsteady stretching surface in presence of thermal radiation. *Alexandria engineering journal*, *53*(3), 737-745.
[17] Haq, R. U., Nadeem, S., Khan, Z. H., & Akbar, N. S. (2015). Thermal radiation and slip effects on MHD stagnation point flow of nanofluid over a stretching sheet. *Physica E: Low-dimensional systems and nanostructures*, *65*, 17-23.
[18] Akbar, N. S., Nadeem, S., Haq, R. U., & Khan, Z. H. (2013). Radiation effects on MHD stagnation point flow of nano fluid towards a stretching surface with convective boundary condition. *Chinese journal of aeronautics*, *26*(6), 1389-1397.
[19] Nagendramma, V., Kumar, R. K., Prasad, P. D., Leelaratnam, A., & Varma, S. V. K. (2016). Multiple slips and radiation effects on Maxwell nanofluid flow over a permeable stretching surface with dissipation. *Journal of nanofluids*, *5*(6), 817-825.
[20] Hayat, T., Qayyum, S., Waqas, M., & Alsaedi, A. (2016). Thermally radiative stagnation point flow of Maxwell nanofluid due to unsteady convectively heated stretched surface. *Journal of molecular liquids*, *224*, 801-810.
[21] Farooq, M., Khan, M. I., Waqas, M., Hayat, T., Alsaedi, A., & Khan, M. I. (2016). MHD stagnation point flow of viscoelastic nanofluid with non-linear radiation effects. *Journal of molecular liquids*, *221*, 1097-1103.
[22] Kumar, R. K., & Varma, S. V. K. (2017). Multiple Slips and Thermal Radiation Effects on MHD Boundary Layer Flow of a Nanofluid Through Porous Medium Over a Nonlinear Permeable Sheet with Heat Source and Chemical Reaction. *Journal of nanofluids*, *6*(1), 48-58.

[23] Das, K. (2015). Nanofluid flow over a non-linear permeable stretching sheet with partial slip. *Journal of the Egyptian mathematical society*, *23*(2), 451-456.
[24] Lee, L. L. (1967). Boundary layer over a thin needle. *The physics of fluids*, *10*(4), 820-822.
[25] Fang, T., Zhang, J., & Zhong, Y. (2012). Boundary layer flow over a stretching sheet with variable thickness. *Applied mathematics and computation*, *218*(13), 7241-7252.
[26] Acharya, N., Das, K., & Kundu, P. K. (2016). Ramification of variable thickness on MHD TiO2 and Ag nanofluid flow over a slendering stretching sheet using NDM. *The European physical journal plus*, *131*(9), 303.
[27] Prasad, K. V., Vajravelu, K., Vaidya, H., & Van Gorder, R. A. (2017). MHD flow and heat transfer in a nanofluid over a slender elastic sheet with variable thickness. *Results in physics*, *7*, 1462-1474.
[28] KiranKumar, R. V. M. S. S., & Varma, S. V. K. (2017). Hydromagnetic Boundary Layer Slip Flow of Nanofluid Through Porous Medium Over a Slendering Stretching Sheet. *Journal of nanofluids*, *6*, 1-10.
[29] Hayat, T., Waqas, M., Alsaedi, A., Bashir, G., & Alzahrani, F. (2017). Magnetohydrodynamic (MHD) stretched flow of tangent hyperbolic nanoliquid with variable thickness. *Journal of molecular liquids*, *229*, 178-184.
[30] Hayat, T., Zubair, M., Waqas, M., Alsaedi, A., & Ayub, M. (2017). Application of non-Fourier heat flux theory in thermally stratified flow of second grade liquid with variable properties. *Chinese journal of physics*, *55*(2), 230-241.
[31] Khader, M. M., & Megahed, A. M. (2013). Numerical solution for boundary layer flow due to a nonlinearly stretching sheet with variable thickness and slip velocity. *The European physical journal plus*, *128*(9), 100.
[32] Devi, S. A., & Prakash, M. (2016). Thermal radiation effects on hydromagnetic flow over a slendering stretching sheet. *Journal of the brazilian society of mechanical sciences and engineering*, *38*(2), 423-431.
[33] Ascher, U. M., Mattheij, R. M., & Russell, R. D. (1994). *Numerical solution of boundary value problems for ordinary differential equations* (Vol. 13). Siam.
[34] Ibrahim, W., Shankar, B., & Nandeppanavar, M. M. (2013). MHD stagnation point flow and heat transfer due to nanofluid towards a stretching sheet. *International journal of heat and mass transfer*, *56*(1-2), 1-9.
[35] Mahapatra, T. R., & Gupta, A. S. (2002). Heat transfer in stagnation-point flow towards a stretching sheet. *Heat and mass transfer*, *38*(6), 517-521.
[36] Bhattacharyya, K. (2013). MHD stagnation-point flow of Casson fluid and heat transfer over a stretching sheet with thermal radiation. *Journal of thermodynamics*. http://dx.doi.org/10.1155/2013/169674